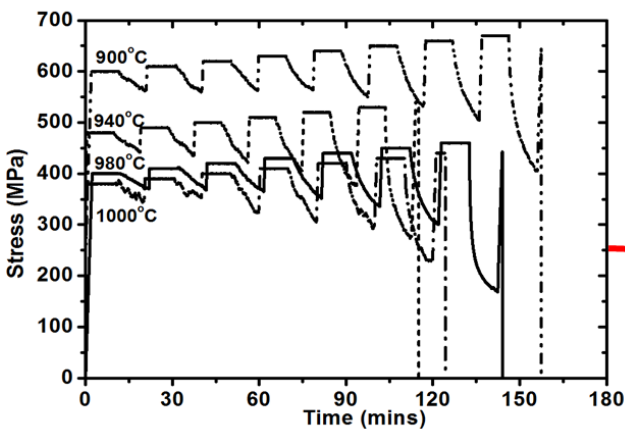


Graphical Abstract



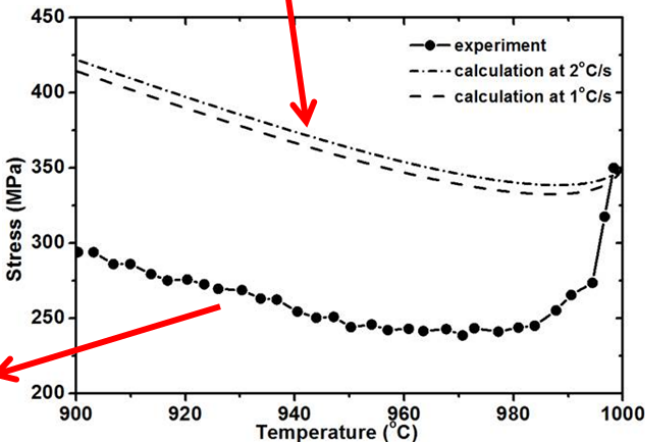
Isothermal stress relaxation tests under displacement control

In-situ cooling test under strain control

Developed Visco-plasticity and relaxation strain constitutive equations:

$$\dot{\epsilon}^{\text{rel}} = 3 \times 10^{-11} \exp\left(-\frac{95000}{8.314 \times T}\right) \exp\left(16 \frac{\sigma}{\sigma_0}\right)$$

$$\dot{\epsilon}^{\text{vp}} = 2.87 \times 10^{-10} \exp\left(-\frac{115706}{8.314 \times T}\right) \exp\left(19 \frac{\sigma}{\sigma_0}\right) t^{-0.405}$$



An experimental investigation into the stress and strain development of a Ni-base single crystal superalloy during cooling from solidification

Chunlei Qiu^{1,2}, Neil D'Souza³, Joe Kelleher⁴, Chinnapat Panwisawas^{1,*}

¹School of Metallurgy and Materials, University of Birmingham, Birmingham B15 2TT, UK

²School of Engineering, Cardiff University, The Parade, Cardiff CF24 3AA, UK

³Rolls-Royce plc, PO Box 31, Derby, DE24 8BJ, UK

⁴ISIS Neutron and Muon Source, Science and Technology Facilities Council, Rutherford

Appleton Laboratory, Harwell Oxford, Didcot OX11 0QX, UK

****Corresponding author: c.panwisawas@bham.ac.uk***

Highlights

- Visco-plasticity occurs during the isothermal relaxation testing under displacement control using in-situ neutron diffractometry.
- An empirical law for the visco-plasticity development during relaxation is purposed to improve predictive capability of process modelling.
- Lattice strain evolution indicates some strain relaxation during the early stage of in-situ cooling, akin to investment casting conditions.
- To replicate the visco-plasticity during cooling from solidification, the isothermal relaxation tests under strain control is anticipated.

An experimental investigation into the stress and strain development of a Ni-base single crystal superalloy during cooling from solidification

Chunlei Qiu^{1,2}, Neil D'Souza³, Joe Kelleher⁴, Chinnapat Panwisawas^{1,*}

¹School of Metallurgy and Materials, University of Birmingham, Birmingham B15 2TT, UK

²School of Engineering, Cardiff University, The Parade, Cardiff CF24 3AA, UK

³Rolls-Royce plc, PO Box 31, Derby, DE24 8BJ, UK

⁴ISIS Neutron and Muon Source, Science and Technology Facilities Council, Rutherford

Appleton Laboratory, Harwell Oxford, Didcot OX11 0QX, UK

**Corresponding author: c.panwisawas@bham.ac.uk*

Abstract

In-situ neutron diffraction has been used to study the stress and strain development in a single crystal Ni-base superalloy (CMSX4) during stress relaxation testing under displacement control mode. It was found that the macroscopic strain is dependent not only on stress and temperature but also on time, suggesting that the overall strain development during stress relaxation is a typical visco-plastic behaviour. The visco-plastic and lattice relaxation strain rates were obtained as best-fit equations from the experimentally measured data encompassing a range of stresses and temperatures. The relaxation lattice strain rate was found to be highly dependent on stress and temperature. It was an order of magnitude smaller than the visco-plastic strain in displacement control mode. An in-situ cooling experiment was also carried out but under strain control mode to simulate the casting condition where the metal solidifies and cools in a rigid ceramic mould. It was found that the stress relaxation was significant in this case and the lattice relaxation dominated visco-plasticity in the early stage

of cooling. These results were compared with the calculations using the currently developed visco-plastic law and some key points are discussed.

Key words: in-situ neutron diffraction; visco-plasticity; in-situ cooling; stress relaxation; lattice strain; nickel-base single crystal superalloys.

1. Introduction

Microstructural control is significant for acquisition of required properties for specific applications. For nickel-base single crystal superalloys, the most important microstructural control is to avoid the formation of stray grains [1] and **sliver** defects [2] during solidification and recrystallisation during subsequent heat treatment. **This is because in all cases** the presence of additional grain boundaries will be detrimental to creep and fatigue properties [3-4]. The former is associated with local casting conditions while the latter is dictated by the localised stress and strain development during solidification and cooling. **On the other hand, surface elemental evaporation during heat treatment has also been shown to promote** recrystallisation [5 - 6]. It is known that stresses could develop during solidification of molten metals and subsequent cooling due to the difference in thermal expansion coefficients of metals and ceramic cores and shells. These stresses can be of a magnitude sufficient to cause plastic yielding of the single crystal superalloys. **The** plastic strain **induced** could be high enough to cause recrystallisation during subsequent heat treatment [7]. Cox et al [7] reported that recrystallisation of a single-crystal superalloy CMSX4 is highly dependent on the degree of plastic strain and temperature at which the strain is introduced. Panwisawas et al [8] further identified the critical plastic strains for recrystallisation of CMSX4 at several high temperatures through experiments. Li et al [9] predicted that the critical plastic strain for recrystallisation to be at least 6% by using a thermal-elastic-plastic model. This kind of research improves the understanding **of** conditions **that could lead to** recrystallisation during post-casting heat treatment. However, these studies are not very helpful in understanding the stress and strain build-up during cooling from solidification. So far, work in this area is generally lacking. Panwisawas et al [10] performed a series of standard creep tests and stress relaxation tests at several high temperatures and found that the creep flow over a range of temperatures is time dependent. They then derived several steady state creep or Norton's

equations to act as a constitutive law of plastic flow to describe the stress and strain evolution during cooling over a wide range of temperatures. Nevertheless, it is noted that the obtained steady state creep equations are not entirely relevant to cooling from solidification as the local solidification/cooling time is much smaller than that considered in creep. Also, the stresses applied in the creep tests (stress control or at a constant stress at a specific temperature) were below the yield stress, **unlike the stresses developed during cooling after solidification that could exceed the yield stress**, according to the calculation using an elasto-plastic model [8, 11].

Our previous work [12] indicates that stress relaxation plays an important role in stress and strain development at a specific temperature. **The role of stress relaxation has been examined in different metals and alloys systems over a wide range of temperatures and applied stresses [13 – 16]. It has been shown that the decay in stress during relaxation follows logarithmic time dependence [15 – 17].** Particularly, relaxation would be significant when the stress in the single crystal superalloys is high. As such, it is important to take stress relaxation into account when we try to develop an understanding on the stress and strain development during cooling. This can be realised by conducting stress relaxation testing over a range of temperatures and stresses. The stress relaxation testing could be performed either under displacement control mode (the length of the metal and the loading train remain constant) or strain control mode (the length of the metal keeps constant). The former mode will involve both elongation and relaxation and as a result the macroscopic strain rate is a combined result of creep (or plastic deformation when stresses are larger than yield strength) and relaxation. In the current study, a series of isothermal stress relaxation tests were performed under displacement control at several high temperatures and different initial stresses. **The main purpose is to develop** constitutive laws to describe the stress and strain development during cooling. It is noted that there are numerous constitutive based modelling laws that have been

developed to simulate creep behaviour of single crystal superalloys [18 - 22]. However, they are not representative for the stress and strain development during cooling from solidification since the assumption of constant stress does not hold true in the continuous cooling case. Also, these models were developed primarily for addressing visco-plasticity in single crystal superalloys to simulate creep behaviour. On the other hand, a number of microstructure-based constitutive models have been developed to describe the visco-plastic flow based upon the dislocation activities and microstructures [23 - 27]. Such microscopic based equations do not assume a constant stress state and thus can be potentially developed to describe the stress and strain development during cooling from solidification. However, they are computationally expensive to be implemented in a macro-solidification model of heat flow. In contrast, the currently proposed experiment-based approach (through a best-fit method) to develop a constitutive law to describe the stress and strain development during cooling is more pragmatic and economical.

An in-situ cooling test from a high temperature was also performed on a single crystal Ni-base superalloy but conducted in strain control mode instead of displacement control mode. The obtained results will be compared with the developed constitutive law. In all of these experiments the neutron diffraction technique will be used, where the lattice strain will be measured. Since the single crystal samples used in this study possess a near-[100] axial orientation (axial orientation was within 5° from [100]), an axial load was applied. As such, a direct correlation between the macroscopic strain and the (200) lattice strain can be obtained because these lattice planes are aligned almost normal to the loading axis. This method permits an in-situ measurement of elastic strain that develops from a change in lattice spacing during cooling.

2. Experimental

2.1 Investment casting of test pieces

Tensile test pieces with a diameter of 5.85 mm and a gauge length of 29 mm of CMSX4 (nominal composition in Table 1) following the design used in [12], have been fabricated using the state-of-the-art investment casting process at the Precision Casting Facility (PCF), Rolls-Royce plc, Derby, UK. Prior to casting, moulds were seeded with CMSX4 with the required orientation to ensure an axial orientation of the single crystals within 5° from [100]. The single crystals were then directionally solidified in a small-bore furnace using a withdrawal rate of 5×10^{-5} m/s. In this manner, the orientation of the seed was conferred on to the test pieces that subsequently solidified; more details are included in [12]. Tensile bars were subject to electro-discharge machining (EDM) at the shoulders and grips, but the gauge length part remained as-cast.

2.2 In-situ neutron diffraction experiments

2.2.1 Isothermal stress relaxation testing

A series of samples were examined during in-situ heating, loading and subsequent relaxation of stress on the ENGIN-X instrument, at the ISIS pulsed neutron facility, Rutherford Appleton Laboratory, Didcot, UK. The setting up of the specimens for in-situ experiments follows the same procedure as has been described in detail elsewhere [12]. The radiant air furnace or so-called mirror furnace [28] was used for heating specimen which was aligned in horizontal direction. A K-type thermocouple was held in contact with the sample to monitor temperature within the gauge region from where the neutron diffraction measurements are made with an accuracy of $(\pm 1^\circ\text{C})$ [29]. The loading axis was horizontal and the rig was positioned to give the longitudinal lattice displacement in one detector and the transverse

lattice spacing in the other. The detectors were fixed at 90° to the incident beam and the data obtained from the full $\pm 15^\circ$ radial detector bank. Isothermal stress relaxation tests were conducted at several high temperatures including 900°C , 940°C , 980°C and 1000°C . In the temperature range of $(900^\circ\text{C} - 1000^\circ\text{C})$, the microstructure comprises of $\gamma + \gamma'$. By using the commercial software, JMatProTM, which employs a multi-component thermodynamic database, Ni-Data developed by ThermoTech UK (Ltd), the phase fraction of γ and γ' were calculated using the equilibrium model [30]. Accordingly, γ fraction was found to vary between 0.30 to 0.36 (γ' fraction varied between 0.68 to 0.62). The samples were heated at a ramping rate of $10^\circ\text{C}/\text{min}$ up to 800°C and thereafter at a rate of $5^\circ\text{C}/\text{min}$ to the set temperatures. At each temperature, a range of initial tensile stresses were used for stress relaxation testing and the stresses were applied at a rate a strain rate of $0.2\% \text{ min}^{-1}$. Specifically, the loading started with a relatively small stress and dwelt at the stress for nine minutes, which was then followed by stress relaxation under displacement control mode for an additional nine minutes. The initial stress was then increased by an increment of 10 MPa from the previous applied initial stress before another dwelling, followed by a stress relaxation test. This process was repeated until the samples failed. The predicted stress ranges derived from previous modelling study of solidification and cooling of simple one-dimensional and three-dimensional bobbin-type geometries has been taken as a reference for the selection of starting stress for each temperature [8, 10]. Prior to loading, each sample was held at each testing temperature for nine minutes for thermal equilibrium and also to get the extensometer stabilised. The detailed loading and stress relaxation testing process are illustrated in Figures 1 and 2. In comparison with a typical creep test where the stress is usually held constant, the stress during relaxation testing generally decreases continuously. Because of this, with the same starting stress and within the same testing timescale Δt , the sample length after creep testing (L_1) is generally larger than that after relaxation testing (L_2).

The difference between the two lengths ($\Delta L = L_1 - L_2$) and thus the difference between two strains are the direct result of stress relaxation, as shown in Figure 1(a). Creep testing is usually performed under stress control mode where the stress σ is kept constant and both the length of specimens (L_A) and the combined length of both specimen and loading train (L_B) will change; see Figure 1(b). The stress relaxation testing could be conducted under either displacement mode or strain mode. Under displacement control mode, both σ and L_A will change but L_B will be kept constant. In this case, any elongation of the specimens will be compensated by the contraction of load trains/arms to keep L_B constant. Under strain control mode, L_A will be strictly kept constant. It is hypothesised that the strain development under either displacement control mode or strain control mode differs from the one conducted with constant stress. Displacement control mode allowed stress relaxation to take place and its contribution to the macroscopic strain will be addressed in this study.

In the current study, the stress relaxation tests were carried out under displacement control mode. During stress relaxation, the lattice spacing (d) decreases and consequently a relaxation strain (ϵ^{rel}) is developed which leads to contraction of the bulk specimen relative to the sample under creep testing where the stress is held constant and there is no such lattice strain development.

The macroscopic strain ϵ developed during stress relaxation testing could be measured by the extensometer attached to the specimens. Further, by measuring the d -spacing by neutron diffraction before and after relaxation testing it is possible to calculate ϵ^{rel} . The neutron diffraction acquisition was made every 3 mins throughout the entire stress dwelling and relaxation process, as shown in Figure 2. The time interval of 3 mins is representative of the local cooling rate under typical casting conditions. Every measurement took 3 mins and three such measurements were made successively throughout a single relaxation test which lasted 9 mins. Therefore, measurement 1 corresponds to a time interval (0 – 3) mins, measurement 2

refers to a time interval (3 – 6) mins and measurement 3 corresponds to a time interval (6 – 9) mins. After heating to each test temperature (900°C, 940°C, 980°C and 1000°C), the sample was held isothermally at that temperature (without application of load) for 9 mins, when three successive measurements were made to determine d_0 and an average was subsequently taken. The integration time for each measurement, i.e. (0 – 3) mins, (3 – 6) mins and (6 – 9) mins is therefore 3 mins.

Consequently, the lattice strain during stress relaxation could be calculated using the following equation:

$$\varepsilon^{\text{rel}} = (d - d_0)/d_0 \quad (1)$$

where d_0 is the starting lattice spacing **before application of load** and d is the d -spacing after stress relaxation in an interval (Δt) **and it must be emphasised that relaxation is occurring during the measurement time.**

With neutron diffraction, both the d -spacing for (100) crystal planes of γ' ($L1_2$) (d_{100}) and that for (200) crystal planes of ($\gamma + \gamma'$) (d_{200}) could be identified. By working out ε^{rel} in different durations and under different temperatures and stress levels, it is possible to derive the dependence of strain rate (or strain) on temperature, stress and time. The strain rate equation is generally in the form of:

$$\dot{\varepsilon}^{\text{vp}} \equiv \dot{\varepsilon}^{\text{vp}}(t, T(t), \sigma) \quad (2)$$

$$\bar{\varepsilon}^{\text{vp}} \equiv \int_0^t \dot{\varepsilon}^{\text{vp}}(t, T(t), \sigma) dt \quad (3)$$

where $\bar{\varepsilon}^{\text{vp}}$ is effective visco-plastic strain or equivalent plastic strain. **However, under displacement control (Figure 1(b)) the two ends of the load train are fixed, but the sample length is not fixed. Therefore, there will also be a change in macroscopic strain (ε)**

accompanying relaxation, although under decreasing stress. By working out $\Delta\epsilon$ in different time durations and under different temperatures and stress levels, it is possible to derive its dependence on temperature, stress and time. This visco-plastic strain is $\Delta\epsilon = \epsilon^{vp}$. Also, it is anticipated that relaxation strain rate is generally in the form of:

$$\dot{\epsilon}^{rel} = \dot{\epsilon}^{rel}(t, T(t), \sigma) \quad (4)$$

It should be emphasised that under constant stress (or stress control), this change in macroscopic strain is attributed to the creep strain.

This kind of analysis has led to development of constitutive laws describing the macroscopic strain and relaxation strain during cooling of a typical nickel-base single crystal superalloy. By adopting an Arrhenius form through a variable separation method, equations of strain rate can be achieved:

$$\dot{\epsilon}^{vp} = A_1 \exp\left(-\frac{E_1}{RT}\right) \exp\left(B_1 \frac{\sigma}{\sigma_0}\right) t^{m_1} \quad (5)$$

$$\dot{\epsilon}^{rel} = A_2 \exp\left(-\frac{E_2}{RT}\right) \exp\left(B_2 \frac{\sigma}{\sigma_0}\right) t^{m_2} \quad (6)$$

where $\dot{\epsilon}^{vp}$ and $\dot{\epsilon}^{rel}$ are the macroscopic strain rate (or visco-plastic strain rate) and relaxation strain rate, respectively, A_1 and A_2 are the pre-exponential constant, E_1 and E_2 are the energy factor, R is the gas constant, T is the temperature, B_1 and B_2 are exponential constants, σ_0 is the 0.2% yield stress.

2.2.2 Continuous cooling testing

In addition to in-situ isothermal testing, an in-situ cooling test was also performed. The sample was heated from room temperature to 1000°C and followed by an isothermal hold for 9 mins. A tensile stress of 350 MPa was applied and the sample was held for a further 9 mins prior to cooling. Cooling was carried out at a nominal rate of 1 °C min⁻¹. During casting, the

metal solidifies and cools in a ceramic mould and hence contraction of metal around a rigid ceramic will place the metal in a state of tension. Hence, for this test, the sample was held under strain control mode to better simulate the real strain development during cooling. The strain control mode uses the reading from an extensometer attached to the sample to counteract the thermal contraction, ensuring that the total strain read from the extensometer remains constant. Strain control gives a better match to the constraint conditions found during casting than the displacement control mode would, since the displacement reading also includes the effect of thermal expansion in the grips, which will not be constant during a cooling test. The initial applied stress of 350 MPa is equivalent to the stress that would have developed in the metal during solidification down to 1000°C [8]. In calculation of the lattice strain using Equation (1), d_0 is the stress-free lattice spacing at a given temperature. This is obtained as a linear best-fit for d_0 measured at 900°C, 940°C, 980°C and 1000°C.

3. Results

3.1 Isothermal stress relaxation

Figure 2 shows the stress development during stress relaxation testing from a series of initial stresses at several different temperatures under displacement control. It can be seen that at each temperature the extent of stress relaxation is significantly dependent on the initial stress level. The higher the initial stress, the more pronounced the stress relaxation. This is consistent with our previous observation on stress relaxation [12]. With successively increased loading and relaxation testing, the strain continually increased until the samples fractured. It is worth emphasising that in the stress relaxation tests, most of the stresses exceeded the yield strength of the material at that temperature; see Figure 2 and Table 2. As such, the measured macroscopic strain is a measure of elongation during stress relaxation.

Since the macroscopic strain is dependent on the stress and testing temperature, for a meaningful comparison between experiments, the applied stress has been normalised by the 0.2 % yield stress σ_0 at each temperature; see Table 3. Accordingly, Figure 3 shows the dependence of macroscopic strain rate on σ/σ_0 within different relaxation durations (3, 6 and 9 mins) at 900°C, 940°C and 1000°C respectively. It can be seen that the macroscopic strain rate increases continuously with σ/σ_0 . At a specific σ/σ_0 and a given temperature, the strain rate decreases with time. This becomes more prominent when σ/σ_0 is larger than 1.28. This time dependence of strain rate suggests that the macroscopic strain that the samples have experienced is visco-plastic in nature. It is also seen that the macroscopic strain rate increases by a factor of 2 - 3 with increasing temperature for a given σ/σ_0 and relaxation time. Based on the best fitting of the experimental data using an Arrhenius type equation, a constitutive equation for the stress and strain development during relaxation in the temperature range [900 – 1000]°C and within a relaxation duration of up to nine minutes **has been** developed;

$$\dot{\epsilon}^{vp} = 2.87 \times 10^{-10} \exp\left(-\frac{115706}{8.314 \times T}\right) \exp\left(19 \frac{\sigma}{\sigma_0}\right) t^{-0.405} \quad (7)$$

According to this equation, it can be further seen that the macroscopic strain developed during relaxation is visco-plastic in nature and that the stress plays a major role in the visco-plastic strain development. Calculations based on this constitutive equation with some specific stresses, times and temperatures have also been performed and compared with the current experimental measurements. The comparison results are shown in Figure 3 with the solid and dotted lines representing the calculations. The calculations were found to be generally in a good agreement with the experimentally measured visco-plastic strain rates although the fit at 900°C becomes worse when σ/σ_0 is larger than 1.28, suggesting that the derived visco-plastic law is valid within the investigated temperature range and time scale.

Owing to stress relaxation, the lattice spacing is expected to decrease during relaxation at 900°C, 940°C, 980°C and 1000°C, respectively and which has been observed. The lattice spacing decreased continuously with increased relaxation time or with continuously decreased stress. Correspondingly, the (200) lattice strain was also found to decrease with stress relaxation; see Figure 4. The dependence of lattice relaxation strain rate on normalised stress (σ/σ_0) and time at several temperatures has also been examined and the results are shown in Table 4 and Figure 5. Importantly, included in Table 4 is the contribution arising from the uncertainty in measurement of the lattice strain. The uncertainty for the (200) lattice strain is defined as, $\Delta\varepsilon(200) = (\Delta d_{200} / d_{200})$, where Δd_{200} is the error in measurement of the (200) lattice spacing. It can be observed unequivocally that the measurement uncertainty is smaller than the measured lattice relaxation strain rates and is less significant at higher stresses. Similar to the case for visco-plastic strain rate, the relaxation strain rate also increases with increased σ/σ_0 but is typically an order of magnitude lower than the visco-plastic strain rate. Moreover, it should be noted that for a given σ/σ_0 and temperature, the visco-plastic strain rate exhibits a monotonic decrease with increased relaxation time, while in the case for the relaxation strain rate, no such a pattern is observed (Figures 3 and 5 and Table 4). To better understand the time dependence of relaxation strain rate, more measurements in longer relaxation durations should be performed. Following the procedure for the visco-plastic strain rate, a best-fit Arrhenius type equation can be derived to describe the evolution of relaxation strain rate within the temperature range of [900 – 1000]°C and time interval of 9 mins;

$$\dot{\varepsilon}^{\text{rel}} = 3 \times 10^{-11} \exp\left(-\frac{95000}{8.314 \times T}\right) \exp\left(16 \frac{\sigma}{\sigma_0}\right) \quad (8)$$

Calculations using this equation at some specific stresses, temperatures and times have been also derived (corresponding to the solid lines in Figure 5). It can be seen that notwithstanding

the temporal dependency being not considered, there is reasonable agreement between the calculated and measured relaxation strain rates. The best-fit is however not as good as in the case of the visco-plastic strain rate where the time dependency was considered.

3.2 In-situ cooling test

Figure 6 shows the stress and lattice strain development during cooling (at 1°C/min) from 1000°C and 350 MPa under strain control mode. It can be seen that in the early stages of cooling, the stress relaxation is significant. The stress decreased by 95 MPa when it cooled down from 1000°C to 988°C and by 77 MPa in the first 5°C cooling, i.e. from 1000°C to 995°C. In the temperature range from 988°C to 957°C, stress relaxation becomes less pronounced with only a slight increase in stress ($\Delta\sigma \sim 3$ MPa). However, upon further cooling from 988°C to 957°C there is an increase in stress governed by the thermal strain. With the stress development during cooling, there is a corresponding change in the (200) lattice strain. The experimental measurement on stress development during cooling is also compared with the calculations derived from the visco-plasticity law that has been developed and described above. The result is shown in Figure 7. There is a similarity in the overall trend of the two curves, i.e. both the calculated and measured show stress relaxation in the early stage of cooling followed by continuous increase of stress as cooling continues. However, there is an order of magnitude difference in the stress between the measured and calculated values. This is consistent with a comparison between one of the current isothermal stress relaxation test under displacement control and one of the previous relaxation tests under strain control mode; see Figure 8. The calculated stress decrease from 1000°C to 990°C is about 5 MPa which is much smaller than the measured value of 85 MPa. This difference arises from the response in stress relaxation during the early stages of cooling. This in turn is dependent on the loading mode used to develop the visco-plasticity law on the one hand and

the deformation mode during cooling on the other. Below 980°C, following initial relaxation a gradual increase in strain is observed. Specifically, in the regime from 957°C to 900°C both the experimentally measured as well as the calculated curves (Figure 7) are nearly parallel to each other and an increment in stress of ~1.5 MPa occurs for every 1°C decrease in temperature.

The stress and strain development of nickel-based single crystal superalloys during cooling can be described as follows:

$$\alpha\Delta T - \Delta\varepsilon = \frac{\Delta\sigma}{E} + \int_0^{\Delta t} \frac{d\varepsilon^{vp}}{dt} dt \quad (9)$$

where α is the thermal expansion coefficient, $\Delta\varepsilon$ is the change in strain during cooling from T to $[T - \Delta T]$ in time interval Δt ($\Delta T > 0$). In the case of free contraction, $\Delta\varepsilon = \alpha\Delta T$, in the case of complete constraint $\Delta\varepsilon = 0$ and for all other cases, $\Delta\varepsilon > 0$.

The measured relaxation in lattice strain $\Delta\varepsilon^{rel}$ and the thermal strain $\alpha\Delta T$ development during cooling from 1000°C to 988°C are shown in Table 5. The uncertainty in the (200) lattice strain ranges between $34 \times 10^{-6} - 36 \times 10^{-6}$ and is also included in Table 5. Again it is clear that the measurement uncertainty is at least five-fold lower than the (200) lattice strain values. Thus, the total relaxation strain in this temperature range is; $\Delta\varepsilon^{rel} = (164 + 531 + 345 + 293) \times 10^{-6} = 1333 \times 10^{-6}$ while the net accumulated thermal strain is; $\alpha\Delta T = (21 + 35 + 61 + 43) \times 10^{-6} = 160 \times 10^{-6}$, where $\alpha = 15.6 \times 10^{-6} \text{ K}^{-1}$). The net measured cumulative decrease in stress in this temperature interval is 95 MPa (i.e., $\Delta\sigma = -95 \text{ MPa}$) according to Figure 7(a). Therefore according to Equation 9, the calculated visco-plastic strain $\int_0^{\Delta t} \frac{d\varepsilon^{vp}}{dt} dt = \alpha\Delta T - \Delta\varepsilon - \frac{\Delta\sigma}{E} = 1.6 \times 10^{-4} - 0 + 95/85000 = 1278 \times 10^{-6}$, where $\Delta\varepsilon = 0$ as the sample cooled under strain control mode and $E = 85 \text{ GPa}$. This compares very well with the measured

relaxation strain $\Delta\varepsilon^{\text{rel}}$ of 1333×10^{-6} . This result further confirms that lattice relaxation has dominated in the stress and strain development at the early stage of cooling. As such, Equation 9 can be re-written as follows,

$$\alpha\Delta T - \Delta\varepsilon = \left[\frac{\Delta\sigma}{E} + \varepsilon^{\text{pl}} \right] + \int_0^{\Delta t} \frac{d\varepsilon^{\text{rel}}}{dt} dt \quad (10)$$

where, ε^{pl} is the time-independent plastic or hardening strain [8, 10, 11] and the visco-plastic term arises primarily from relaxation of the elastic strain, i.e. $\frac{d\varepsilon^{\text{vp}}}{dt} \sim \frac{d\varepsilon^{\text{rel}}}{dt}$.

It is also noted that on the onset of cooling (at 1000°C), $\sigma = 350$ MPa, $\varepsilon^{\text{el}} = 4500 \times 10^{-6}$ and $\varepsilon^{\text{pl}} = 731 \times 10^{-6}$ (according to Figure 7(b)). Given that relaxed lattice strain $\Delta\varepsilon^{\text{rel}}$ during cooling from 1000°C to 988°C is 1333×10^{-6} , this means $\sim 30\%$ ($= \Delta\varepsilon^{\text{rel}} / \varepsilon^{\text{el}}$) of the elastic strain has been converted into plastic strain during relaxation. Also at 1000°C and for $\sigma = 350$ MPa, the elastic strain constitutes almost 86% of the total strain ($= \varepsilon^{\text{el}} / (\varepsilon^{\text{el}} + \varepsilon^{\text{pl}}) = 4500 / (4500 + 731)$). Beyond initial relaxation, between 900°C and 980°C, since $\sigma < \sigma_0$ only elastic deformation occurs since the visco-plastic contribution according to Equation 7 is at least an order of magnitude smaller. Therefore, according to Equation 10, $\Delta\sigma$ is around 1.5 MPa for every 1°C decrease in temperature ($\varepsilon^{\text{pl}} = 0$). **Based on the results, it is obvious that the evolution of stress is related to the decrease in temperature and also the relaxation that is occurring simultaneously, especially for low cooling rates (1 K/min). During initial cooling in the temperature range of (1000°C – 988°C), the decrease in stress principally arises from relaxation effects, as the ratio of relaxation strain to thermal strain is at least close to six-fold. In the temperature range of (988°C – 957°C) the increase in stress is marginal, as relaxation is almost countered by the development of thermal strain. In the temperature range of (957°C – 900°C), the thermal strain dictates the increase in stress.**

4. Discussion

The current experimental results have clearly demonstrated that the development of macroscopic strain during stress relaxation testing and cooling of single crystal nickel-base superalloys is time dependent and thus visco-plastic in nature. Also, according to the visco-plasticity law developed based on testing under displacement control (Equation 7), the stress dependence of visco-plasticity is more pronounced than the time dependence. Therefore, under these conditions, when the accumulated stress exceeds the yield stress during cooling at a specific temperature, **time-dependent elongation** would be dominant in order to compensate **for** the thermal strain according to Equation 9, if the sample was constrained.

The calculations based on the developed constitutive equation for several stresses and temperatures within a certain timescale were found to be in good agreement with the current isothermal experimental result but show significant deviation from the in-situ cooling experimental measurements. The relaxation in stress is **significantly** greater under strain control than under displacement control in the early stages of cooling (**Figure 6**) and **requires further investigation**. Further investigation in the micro-mechanisms is required to better understand this issue. It is also demonstrated that in the case of cooling under strain control mode, only lattice relaxation contributes to visco-plasticity and **time-dependent elongation** should be ignored (Equation 10). This is in contrast to the contribution of lattice relaxation to visco-plasticity under displacement control mode where the lattice relaxation strain only contributes around 10 % of the total visco-plasticity (according to Figures 3 and 5, the lattice relaxation strain is one order of magnitude smaller than visco-plastic strain over a range of temperatures). This result suggests that relaxation test under displacement control has underestimated the role of relaxation in visco-plasticity development under casting condition that is akin to strain control. This is very important for selection of loading modes for isothermal experiments (stress, displacement and strain control) to develop the visco-plastic

law for stress and strain development of nickel-base superalloys during cooling from high temperatures. It is obvious that the conventional method of constant stress is incorrect, as it neglects relaxation. The choice of displacement control to allow for relaxation to decrease stress is also incomplete. In the absence of a rigid constraint, **time-dependent elongation** will dominate over relaxation when actual stress is larger than yield stress ($\sigma > \sigma_0$), which leads to an under-estimation of visco-plasticity and thus is not representative of casting conditions. During casting the contraction of the metal is highly constrained by the ceramic mould and internal core due to the significant difference in the thermal expansion coefficients of the metal and ceramic (by an order of magnitude) [10, 11]. Therefore, isothermal experiments under strain control mode would be thus the most appropriate approach in developing visco-plastic law to describe the stress and strain development during cooling after solidification. Therefore, our future work will focus on performing a series of stress relaxation tests under strain control mode over a range of temperatures to simulate the visco-plasticity during the cooling process and to improve the understanding of stress and strain development during cooling from solidification. Nevertheless, it is important to emphasise that the currently developed constitutive law is better than the usually adopted constitutive equations developed for creep in predicting the stress and strain development during cooling as it has taken into account the stress relaxation factor.

Moreover, the current observation of significant stress drop in the beginning of in-situ cooling test is significant for the stress and strain control for nickel-base single crystal superalloys in the early stage of cooling after solidification. According to Panwisawas et al's modelling and analysis [8], the plasticity needed for recrystallisation is induced during the early stages of cooling. As such, if measures could be taken to promote stress relaxation in the early stage of cooling from solidification, we may avoid excessive build-up of plasticity that would be high enough to trigger recrystallisation during post-casting heat treatment.

5. Conclusions

- The macroscopic strain development of a nickel-base single crystal superalloy during stress relaxation was found to be visco-plastic for the range of stresses ($\sigma > \text{yield stress}$) and the temperature range (900°C to 1000°C) in this study.
- A constitutive equation has been developed based on isothermal stress relaxation tests under displacement control mode to describe the visco-plasticity development during relaxation.
- Lattice relaxation dominated the visco-plastic strain development in the early stage of cooling when the samples were tested under strain control mode that is equivalent to casting conditions.
- The calculation based on the currently developed visco-plasticity equation underestimates the role of relaxation in stress and strain development during early stage of cooling.
- Stress relaxation under strain control mode is at least two-fold greater than that occurring under displacement control mode and the former is more appropriate for determining the visco-plastic response under the conditions studied.

Acknowledgements

The authors acknowledge the help of Mr. Kevin Goodwin, Martin Perry and Dean Welton from the Precision Casting Facility (PCF) for the manufacture of the tensile test pieces and fixtures for the Instron machine.

References

- [1] T.D. Anderson, J.N. DuPont, T. DebRoy, Origin of stray grain formation in single-crystal superalloy weld pools from heat transfer and fluid flow modeling, *Acta. Mater.* 58 (2010) 1441–1454.
- [2] J. W. Aveson, P.A. Tennant, B. J. Foss, B. Shollock, H. J. Stone, N. D'Souza, On the origin of sliver defects in single crystal investment castings, *Acta. Mater.* 61 (2013) 5162–5171.
- [3] J. Meng, T. Jin, X.F. Sun, Z.Q. Hu, Effect of surface recrystallization on the creep rupture properties of a nickel-base single crystal superalloy, *Mater. Sci. Eng. A* 527 (2010) 6119–6122.
- [4] J.J. Moverare, S. Johansson, R.C. Reed, Deformation and damage mechanisms during thermal–mechanical fatigue of a single-crystal superalloy, *Acta. Mater.* 57 (2009) 2266–2276.
- [5] H. Wang, N. D'Souza, S.X. Zhao, D. Welton, N. Warnken, R.C. Reed, Effects of elemental vaporization and condensation during heat treatment of single crystal superalloys, *Scripta. Mater.* 78–79 (2014) 45–48.
- [6] N. D'Souza, D. Welton, G.D. West, I.M. Edmonds, H. Wang, On the roles of oxidation and vaporization in surface micro-structural instability during solution heat treatment of Ni-base superalloys, *Metall. Mater. Trans. A* 45 (2014) 5968–5981.
- [7] D.C. Cox, B. Roebuck, C.M.F. Rae, R.C. Reed, Recrystallisation of single crystal superalloy CMSX-4, *Mater. Sci. Technol.* 19 (2003) 440–446.
- [8] C. Panwisawas, H. Mathur, J.-C. Gebelin, D. Putman, C.M.F. Rae, R.C. Reed, Prediction of recrystallization in investment cast single-crystal superalloys, *Acta. Mater.* 61 (2013) 51–66.
- [9] Z.L. Li, J.C. Xiong, Q.Y. Xu, J.R. Li, B.C. Liu, Deformation and recrystallization of single crystal nickel-based superalloys during investment casting, *J. Mater. Proc. Technol.* 217 (2015) 1–12.

[10] C. Panwisawas, Modelling and Prediction of Recrystallisation in Single Crystal Superalloys, PhD Thesis, University of Birmingham, 2013.

[11] C. Panwisawas, J.-C. Gebelin, R.C. Reed, Analysis of the mechanical deformation arising from the investment casting of directionally solidified and single crystal superalloys, *Mater. Sci. Technol.* 29 (2013) 843 – 853.

[12] N. D'Souza, J. Kelleher, C.L. Qiu, S.Y. Zhang, S. Gardner, R. E. Jones, D. Putman, C. Panwisawas, The role of stress relaxation and creep during high temperature deformation in Ni-base single crystal superalloys-Implications to strain build-up during directional solidification, *Acta. Mater.* 106 (2016) 322 - 332.

[13] M. Dupeux, J. Henriot, M. Ignat, Tensile stress relaxation behaviour of Ni-based superalloy single crystals between 973 and 1273K, *Acta Metall.*, 35 (1987) 2203 – 2212.

[14] H. Wang, B. Clausen, C. N. Tome, P. D. Wu, Studying the stress relaxation and creep on lattice strain evolution of stainless steel under tension, *Acta Mater.* 61 (2013), pp. 1179 – 1188.

[15] P. Feltham, Stress relaxation in alpha-iron at low temperatures, *Phil. Mag.* 6:67 (1961) 847 – 850.

[16] B. Jakobson, H. F. Poulsen, U. Lienert, J. Bernier, C. Gundlach, W. Pantleon, Stability of dislocation structures in copper towards stress relaxation investigated by high angular resolution 3D X-ray diffraction, *Phys. Stat. Sol. A* 206 (2009) 21 – 30.

[17] F. R. N. Nabarro, The time constant for logarithmic creep and relaxation, *Mat. Sci. Eng.* A 309 – 310 (2001) 227 – 228.

[18] J.L. Chaboche, A review of some plasticity and viscoplasticity constitutive theories, *Int. J. Plast.* 24(10) (2008) 1642–1693.

- [19] J.-B. le Graverend, J. Cormier, F. Gallerneau, P. Villechaise, S. Kruch, J. Mendez, A microstructure-sensitive constitutive modeling of the inelastic behavior of single crystal nickel-based superalloys at very high temperature, *Int. J. Plast.* 59 (2014) 55–83.
- [20] J. Cormier, G. Cailletaud, Constitutive modeling of the creep behavior of single crystal superalloys under non-isothermal conditions inducing phase transformations, *Mater. Sci. Eng. A* 527 (2010) 6300-6312.
- [21] M. McLean, B.F. Dyson, Modeling the Effects of Damage and Microstructural Evolution on the Creep Behavior of Engineering Alloys, *J. Eng. Mater. Technol.* 122 (2000) 273-278.
- [22] B.F. Dyson, Microstructure based creep constitutive model for precipitation strengthened alloys: Theory and application, *Mater. Sci. Technol.* 25 (2009) 213–220.
- [23] G. Cailletaud, A micromechanical approach to inelastic behaviour of metals, *Int. J. Plast.* 8 (1992) 55-73
- [24] M.F. Ashby, B.F. Dyson, Creep damage mechanics and micromechanisms, in: S. R. Valluri et al (Eds.), *Advances in Fracture Research*, Pergamon Press, 1984, pp. 3–30.
- [25] A. Ma, D. Dye, R.C. Reed, A model for the creep deformation behaviour of single-crystal superalloy CMSX-4, *Acta. Mater.* 56 (2008) 1657 – 1670.
- [26] J. Coakley, D. Dye, H.C. Basoalto, Creep and creep modelling of a multimodal nickel-base superalloy, *Acta. Mater.* 59 (2011) 854 – 863.
- [27] Z. Zhu, H.C. Basoalto, N. Warnken, R.C. Reed, A model for the creep deformation behaviour of nickel-based single crystal superalloys, *Acta. Mater.* 60 (2012) 4888 – 4900.

- [28] I.F. Bailey, A review of sample environment in neutron scattering, *Z. Kristallogr.* 218 (2003) 84–95
- [29] J. Coakley, R.C. Reed, J.L.W. Warwick, K.M. Rahman, D. Dye, Lattice strain evolution during creep in single-crystal superalloys, *Acta Mater.* 60 (2012) 2729 – 2738.
- [30] JMatPro Ni module (Version 2.0), Sente Software, Guildford, UK (2002).

Table 1: The nominal compositions (in wt. %) of CMSX4 single-crystal superalloy.

Cr	Co	Mo	Re	W	Al	Ti	Ta	Hf	Ni
6.5	9	0.6	3	6	5.6	1	6.5	0.1	Balance

Table 2: 0.2% yield strengths of CMSX4 single-crystal superalloy at different temperatures.

T (°C)	900	940	980	1000
σ_0 (MPa)	500	400	342	325

Table 3: Different applied stresses at different temperatures and corresponding σ/σ_0 for relaxation testing.

σ (MPa) - 1000°C	σ (MPa) - 940°C	σ (MPa) - 900°C	σ / σ_0
390	480	600	1.2
400	490	620	1.232
410	500	630	1.257
-	510	640	1.278
420	520	650	1.297
430	530	660	1.323

Table 4: Relaxation strain rate as a function of σ/σ_0 at different temperatures within different relaxation durations. Also included is the contribution from measurement uncertainty.

σ / σ_0	$\frac{d\epsilon^{rel}}{dt}$ ($10^{-7}/s$) within 3 mins			$\frac{d\epsilon^{rel}}{dt}$ ($10^{-7}/s$) within 6 mins			$\frac{d\epsilon^{rel}}{dt}$ ($10^{-7}/s$) within 9 mins		
	1000°C	940°C	900°C	1000°C	940°C	900°C	1000°C	940°C	900°C
1.2	4.6 ± 1.6 1.2	7.9 ± 2.0 2.0	3.7 ± 2.0 2.0	5.95 ± 1.2 1.2	7.9 ± 1.0 1.0	6.3 ± 1.0 1.0	-	7.0 ± 0.7 0.7	7.4 ± 0.7 0.7
1.232	11.6 ± 1.4 1.4	5.8 ± 1.9 1.9	7.0 ± 1.8 1.8	11.0 ± 0.7 0.7	9.5 ± 1.0 1.0	8.3 ± 0.9 0.9	12.5 ± 0.4 0.4	9.7 ± 0.6 0.6	9.78 ± 0.5 0.5
1.257	13.7 ± 1.3 1.3	6.7 ± 1.9 1.9	11.6 ± 1.7 1.7	18.3 ± 0.6 0.6	12.4 ± 0.9 0.9	12.5 ± 0.8 0.8	17.8 ± 0.4 0.4	11.8 ± 0.6 0.6	12.5 ± 0.6 0.6
1.278	-	11.9 ± 2.8 2.8	15.6 ± 1.6 1.6	-	25.0 ± 0.8 0.8	17.7 ± 0.8 0.8	-	20.8 ± 0.6 0.6	16.3 ± 0.5 0.5
1.297	34.5 ± 1.2 1.2	32.1 ± 1.6 1.6	20.8 ± 1.6 1.6	33.9 ± 0.6 0.6	35.1 ± 0.8 0.8	26.0 ± 0.8 0.8	27.1 ± 0.4 0.4	29.1 ± 0.5 0.5	23.3 ± 0.5 0.5

Table 5: Development of lattice strain and thermal strain during cooling between 1000°C and 988°C. Also included is the contribution from measurement uncertainty.

Strain x 10 ⁶	(1000-997)°C	(997-994)°C	(994-991)°C	(991-988)°C
Lattice strain	164 ± 36	531 ± 34	345 ± 35	293 ± 35
Thermal strain	21	35	61	43

Figure

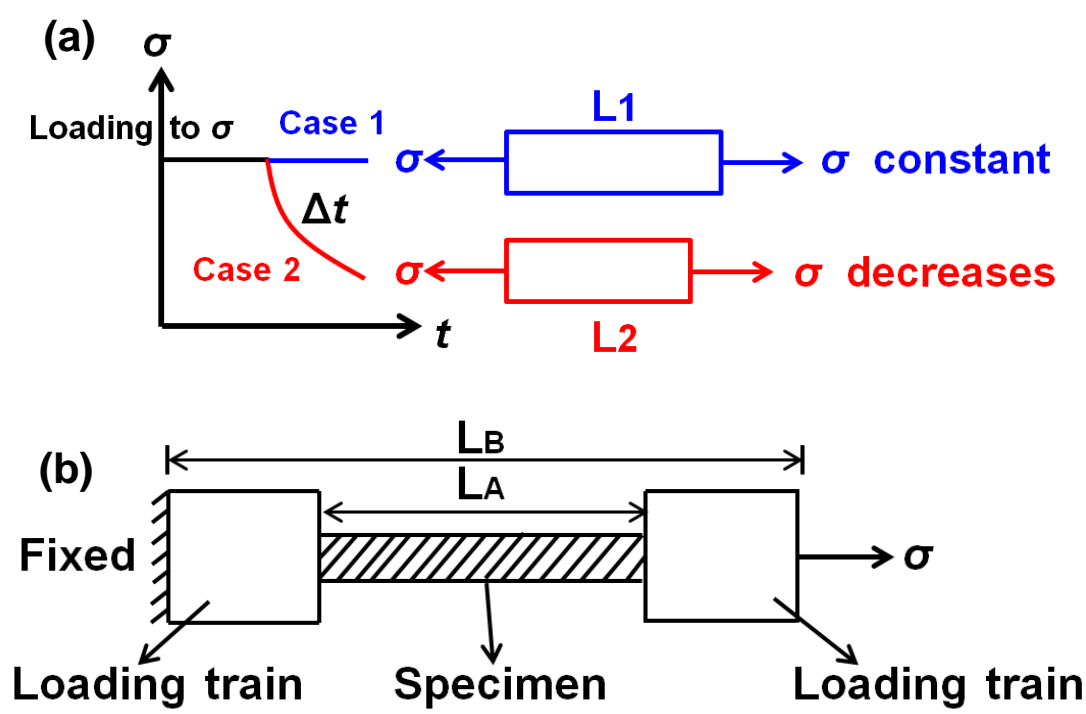


Figure 1: (a) Schematic illustration of the difference between creep test (case 1, constant stress; when σ is beyond yield strength, it will be tensile test at a constant stress) and stress relaxation test (case 2, decreasing stresses); L1 and L2 are the lengths of samples after creep and relaxation testing within the same time scale Δt from the same original sample length L_0 ; (b) Schematic illustration of the setting up of specimens and loading unit.

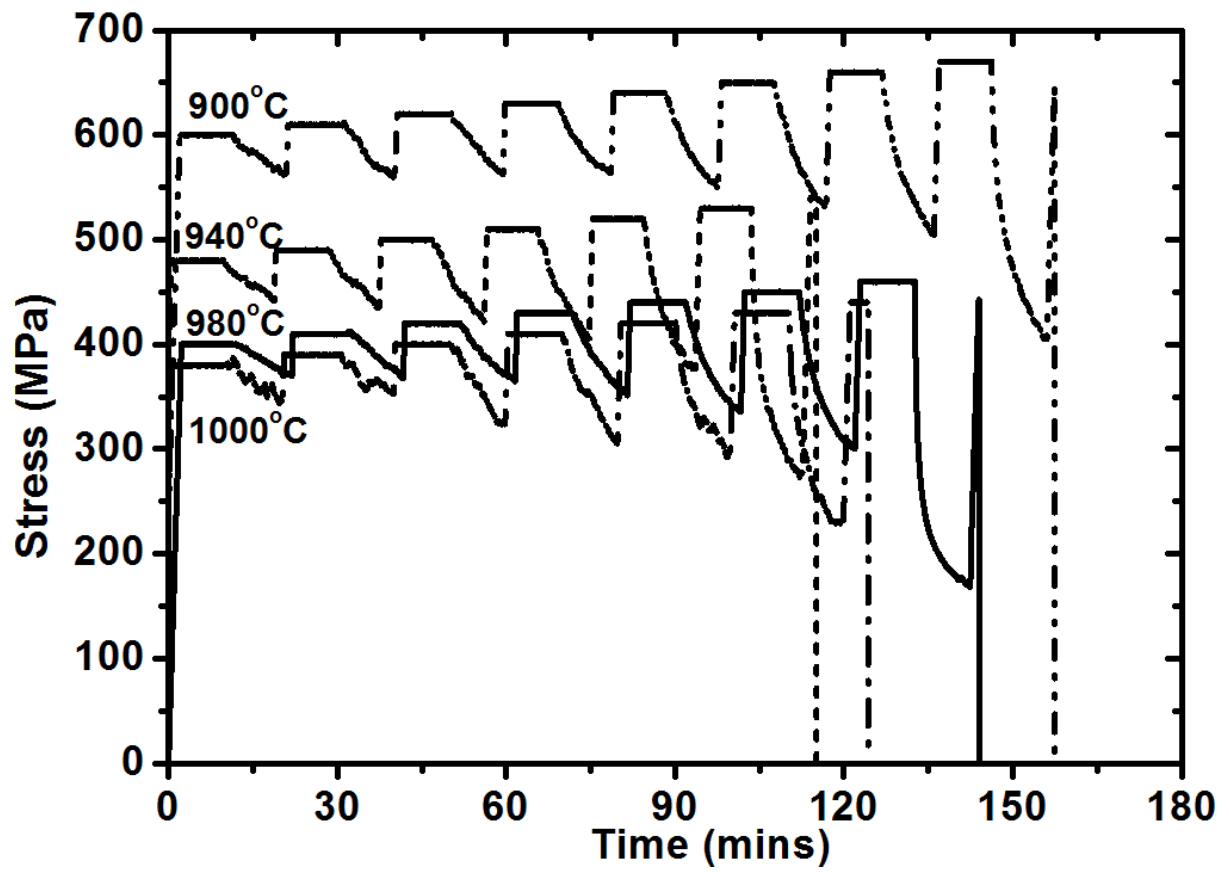


Figure 2: Stress development during stress relaxation tests under displacement control over a series of stresses at (a) 900°C; (b) 940°C; (c) 980°C; (d) 1000°C.

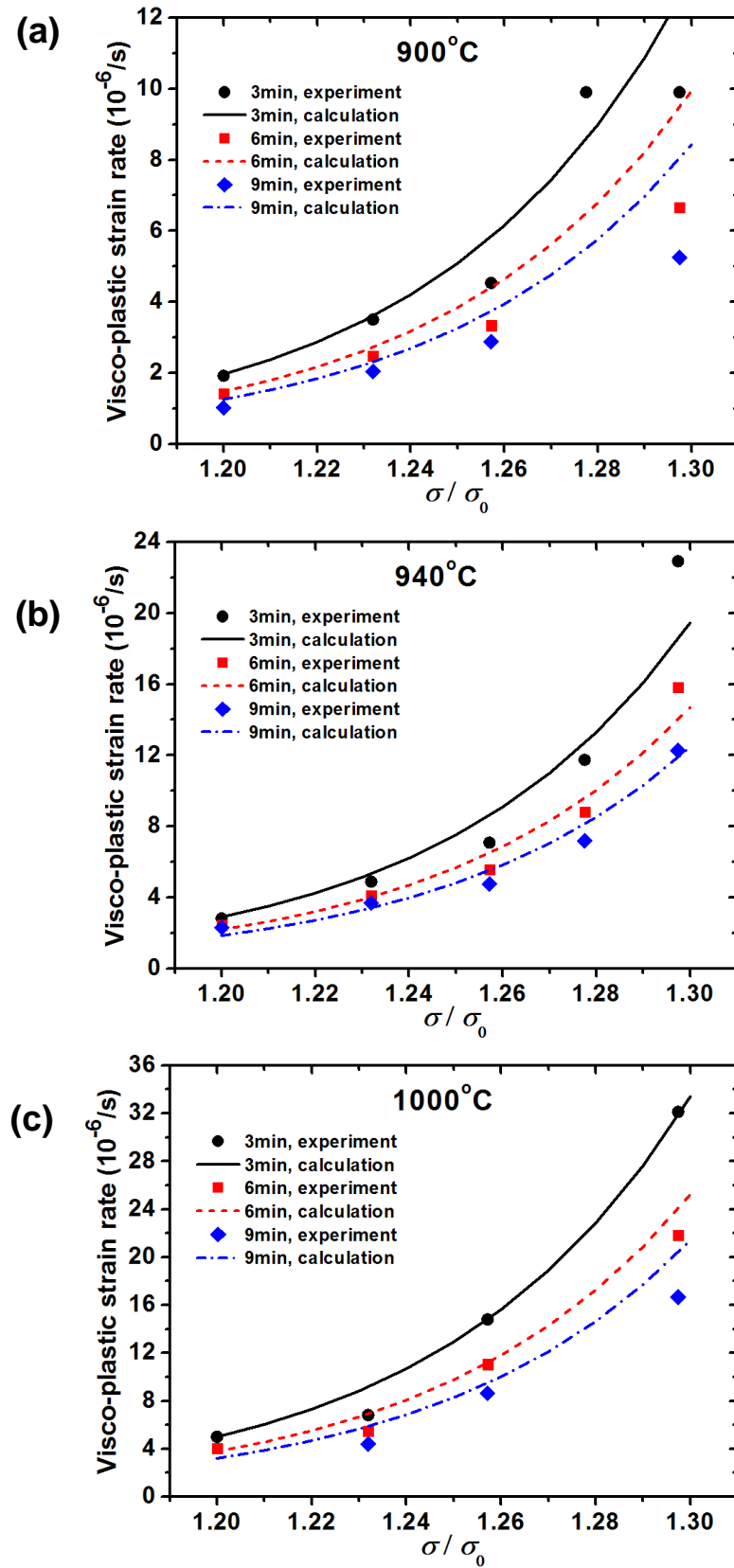


Figure 3: Dependence of visco-plastic strain rate on stress and time during relaxation testing at several temperatures (a) 900°C; (b) 940°C; (c) 1000°C. The fitting lines here are from the proposed visco-plastic law.

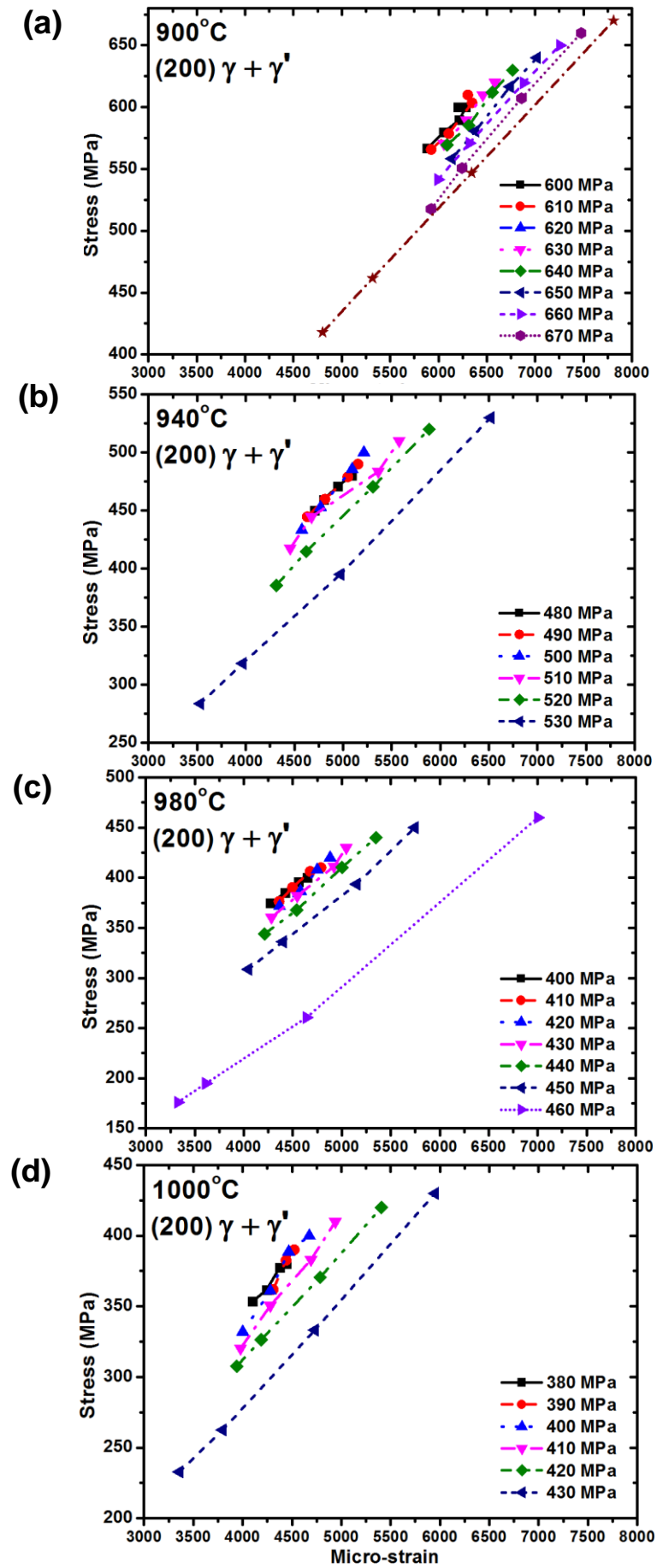


Figure 4: Dependence of (200) lattice strain on stress development during relaxation testing at different temperatures under displacement control.

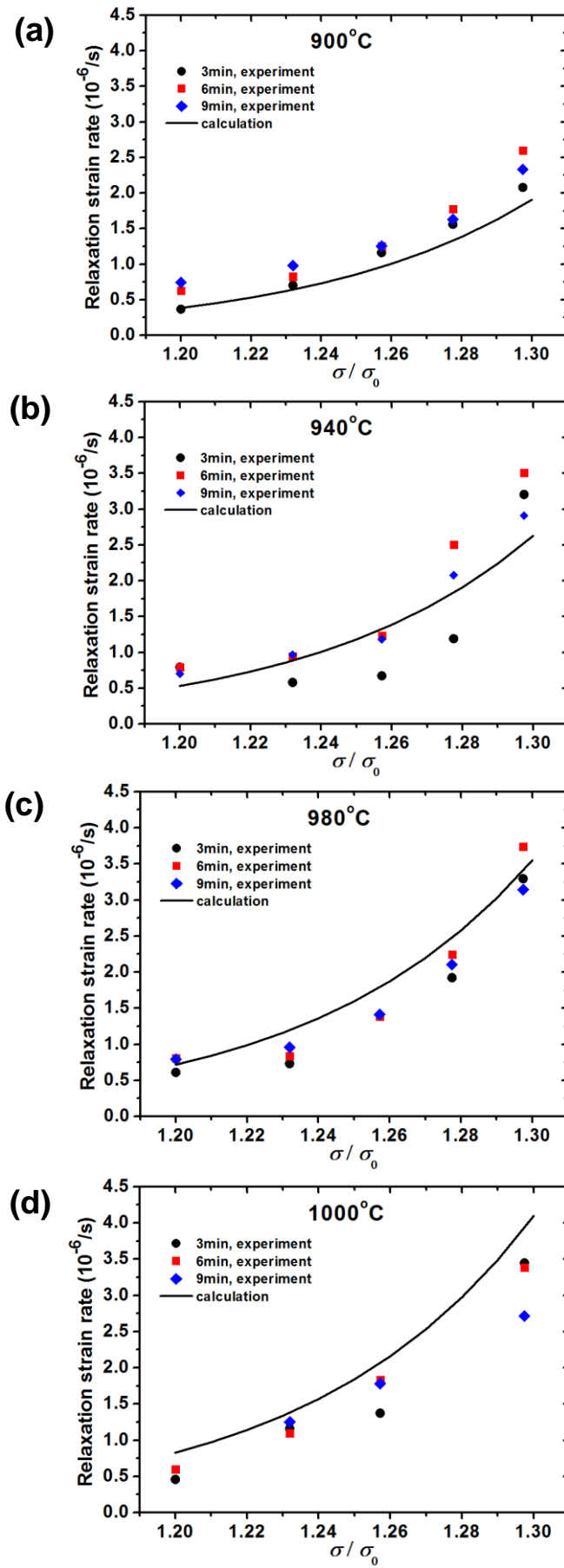


Figure 5: Dependence of relaxation strain rate on stress and time at several temperatures (a) 900°C; (b) 940°C; (c) 980°C; (d) 1000°C. The calculations are from the proposed relaxation law.

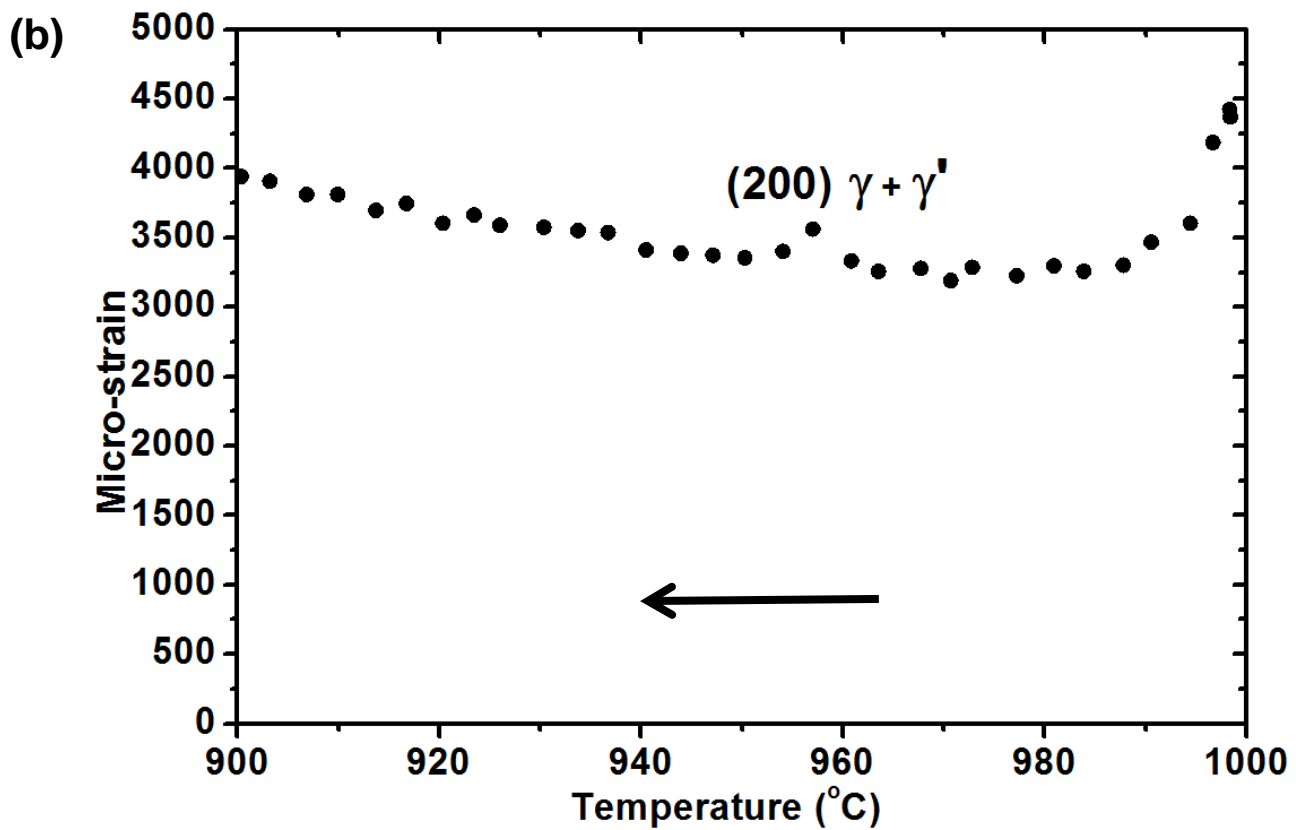
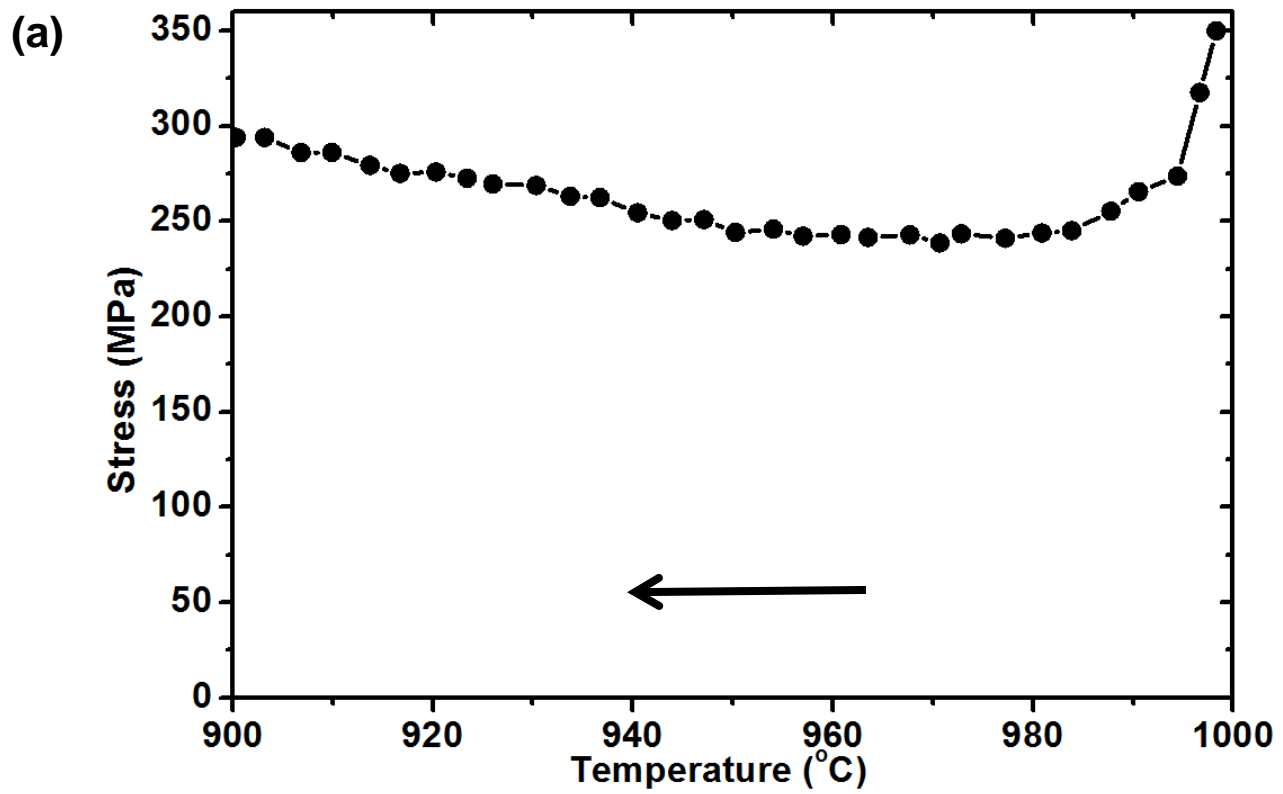


Figure 6: Stress and lattice strain evolution during cooling at 1°C/min from 1000°C under strain control mode.

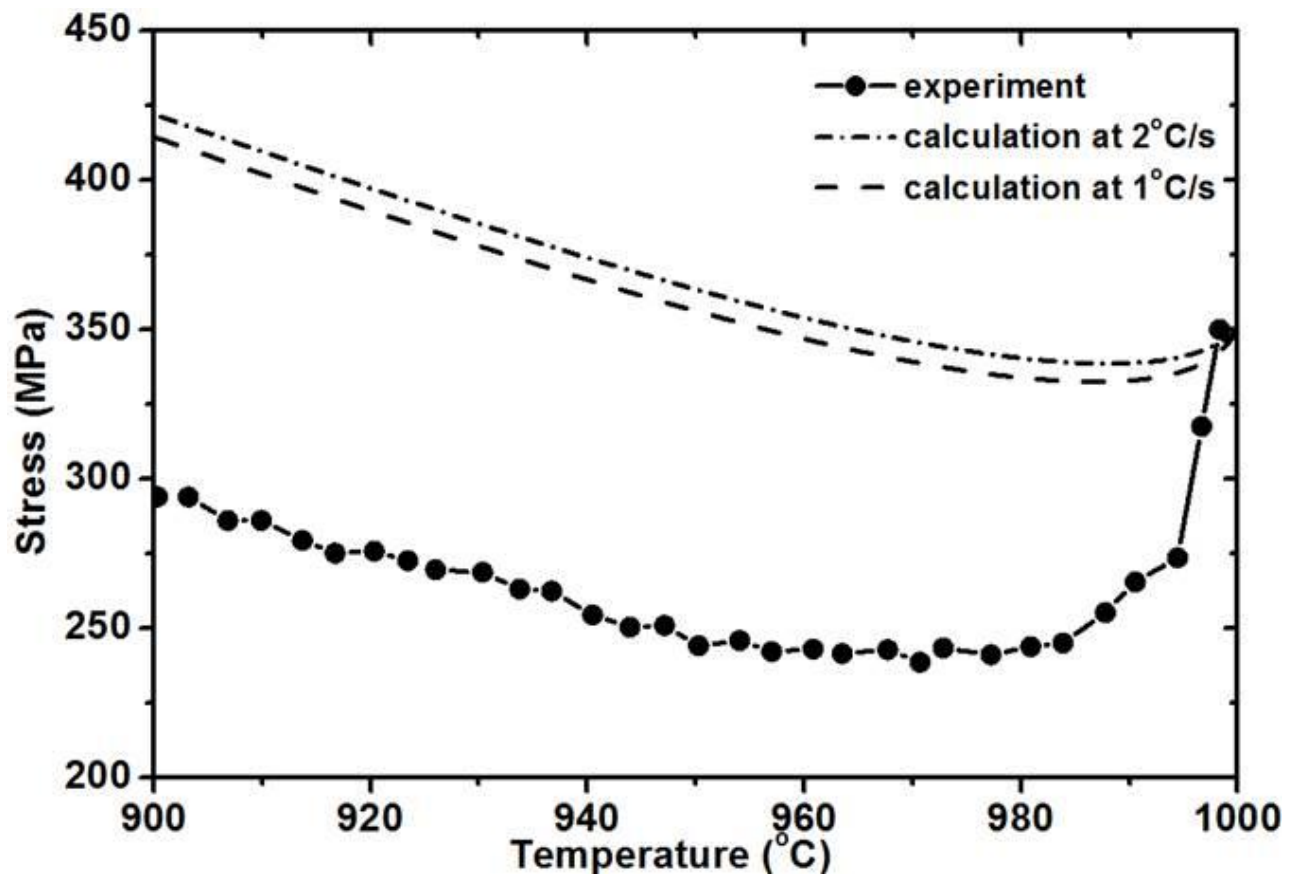


Figure 7: Comparison between calculated and measured stress evolution during cooling from 1000°C.

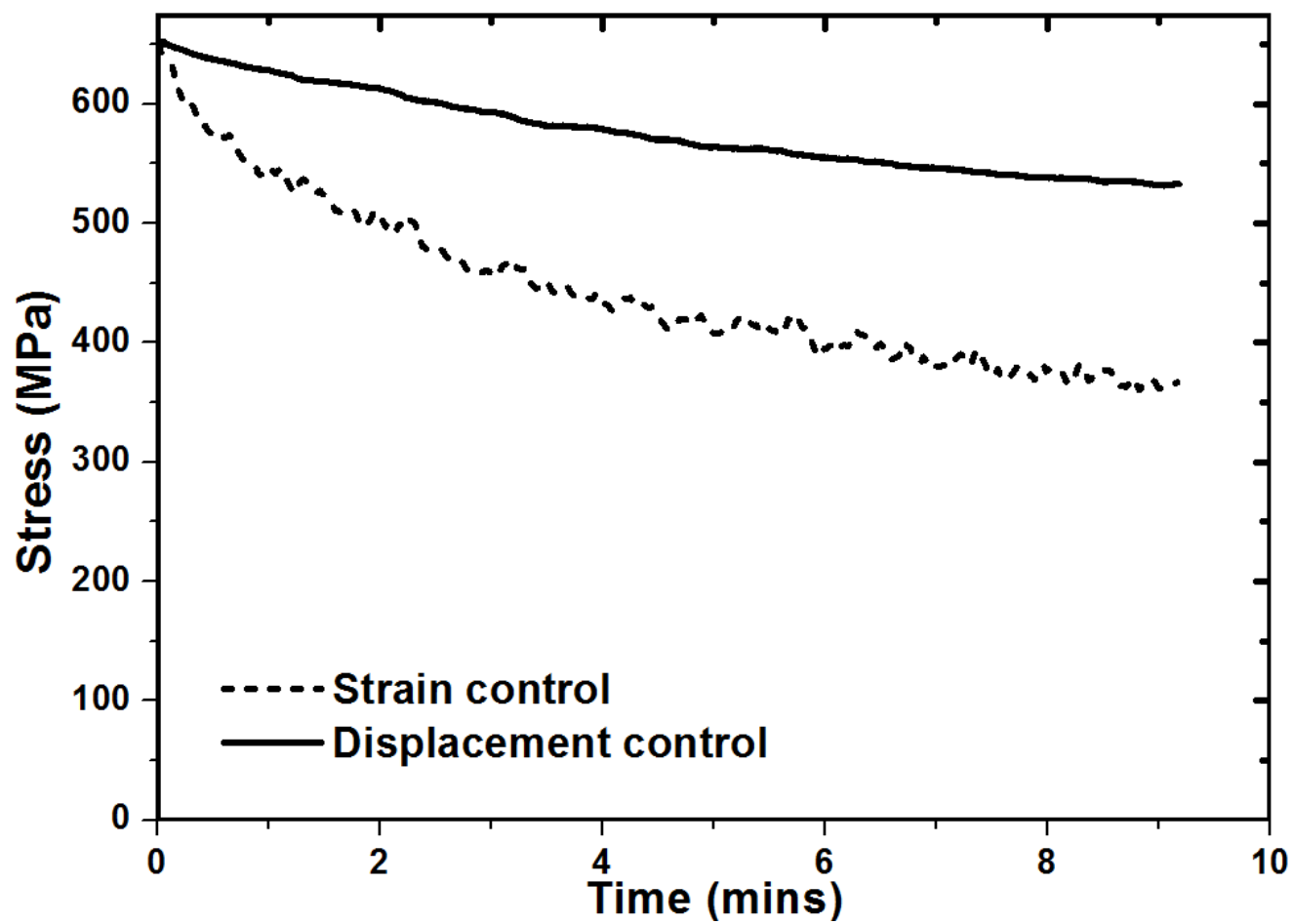


Figure 8: Comparison of stress relaxation under displacement control and strain control. The two relaxation tests were performed at 900°C and started with a stress of 650MPa